Multi-Functional V2G Interface With Improved Dynamic Response for Shunt Compensation

Arpitkumar J. PATEL and Amit V. SANT

***Abstract*—This paper proposes a multi-functional vehicle -to-grid (M-V2G) interface based on the new fundamental active current (FAC) extraction method for shunt compensation (SC) with enhanced dynamic response. The M-V2G operates in four modes, namely (A) active power injection (API), (B) API and SC, (C) API and partial SC, and (D) SC. The proposed FAC extraction method involves processing the *d*-axis current of non-linear load through the cascaded band-stop filter. The resulting signal comprises a dc and an ac component with six times the fundamental frequency. For balanced currents, FAC is derived as the value of this signal sampled at the absolute peak value of its derivative. For unbalanced load currents, FAC extraction considers (i) the average of six consecutive samples, or (ii) inclusion of an additional BSF with a center frequency corresponding to the 6th harmonic is included. The second option provides a faster dynamic response. M-V2G interface is controlled based on the FAC and commanded API. The proposed technique ensures accurate FAC estimation without complex computations, as evident from the pseudo-code and experimental studies. Further, the experimental results confirm its effectiveness, feasibility, and practical viability. The M-V2G interface with the proposed FAC estimation scheme increases power quality and VA utilization of the V2G interface.**

***Index Terms*—Battery, electric vehicles, multi-functional control, shunt compensation, vehicle-to-grid (V2G).**

I. Introduction

ELECTRIC vehicles (EVs) have emerged as a cleaner alternative to internal combustion (IC) based vehicles. On the other hand, for the utility, the rising number of EVs poses challenges of increased energy demand, network congestion, and power quality (PQ) issues [1]−[3]. The grid-interfaced EV charger requires an ac-dc converter at the grid side. Using a diode-based ac-dc converter at the input stage of an EV charger may be economical. However, the diode rectifier injects harmonic currents into the grid. The impact of EV charging stations on grid PQ is discussed in [4]−[5]. Further, the increasing usage of power converters in industrial, domestic, and commercial sectors deteriorates the PQ by harmonic current injection into the grid. The PQ issue is further compounded by the ever-increasing nonlinear loads [6]. The harmonic currents in the grid are responsible for the increased line losses, line congestion, mal-operation of control and protective equipment, and reduced power transfer capability [7]. PQ issues are prone to increase upon the installation of EV charging stations on a larger scale. Hence, mitigating the PQ issues at the charging station is necessary. [2] and [8] suggest the installation of a distributed static compensator (DSTATCOM) and shunt active power filter (SAPF) at the charging station to nullify current harmonics. In EV chargers, using pulse width modulated (PWM) rectifiers in place of diode-based rectifiers is beneficial with respect to the PQ concerns as it offers a unity power factor and reduces total harmonic distortion (THD) at the grid end. Moreover, the EV charger can facilitate bi-directional power flow with PWM rectifiers, provided that the bi-directional dc-dc converter is employed. This enables EV chargers to perform vehicle-to-grid (V2G) operations to offer ancillary services to the grid. The V2G operation refers to the power flow from the EV to the grid, while the grid-to-vehicle (G2V) operation refers to charging the EV battery from the grid.

EV chargers can operate in V2G mode and perform active power injection (API) to meet the active power demand of load (APDL) [9]. Such operation may not always result in complete utilization of the interface's VA capacity. Moreover, the issue of PQ degradation due to other nonlinear loads at the station premises needs to be addressed. The IGBT-based ac-dc interface of the EV charger holds a power structure similar to that of SAPF. This enables the utilization of the V2G interface to mitigate the harmonic currents drawn by the other loads at the station premises. The implementation, however, necessitates additional control loops. The multi-functional control of V2G ensures the implementation of requisite shunt compensation (SC) and/or traditional charging or API operations. Hence, for increased VA utilization and addressing current related PQ issues, a multifunctional-V2G (M-V2G) interface can be controlled to perform API and SC, which can compensate for the harmonic currents and reactive power demand of load (RPDL). For providing SC through the V2G interface, estimation of the fundamental active component (FAC) of load current is essential. This paper introduces a new FAC extractor (FACE) that offers computational simplicity, fast dynamic response, and accurate FAC estimation, even under unbalanced load conditions. The proposed M-V2G interface operates in four distinct modes, namely, (A) API, (B) API and SC, (C) API with partial SC, and (D) SC only. The proposed technique enhances VA

Manuscript received November 20, 2024; revised February 28, 2025; accepted March 27, 2025. Date of publication June 30, 2025; date of current version April 18, 2025. No funding was received to assist with the preparation of this manuscript. *(Corresponding author: Arpitkumar J. Patel.)*

Both authors are with the Department of Electrical Engineering, School of Energy Technology, Pandit Deendayal Energy University, Gandhinagar, India (e-mail: arpit.pphd20@sot.pdpu.ac.in; amit.sant@sot.pdpu.ac.in).

Digital Object Identifier 10.24295/CPSSTPEA.2025.000016

TABLE I
COMPARATIVE ANALYSIS OF M-V2G INTERFACE

Operating Modes	[9]	[11]	[12]	[13]	[14]	[15]	Proposed
API	✓	✓	✓	✗	✗	✗	✓
API and HCM	✗	✗	✗	✗	✓	✓	✓
API and RPC	✗	✗	✓	✗	✓	✓	✓
API and Partial SC	✗	✗	#	✗	✗	✗	✓
SC Only	✗	✗	✓	✓	✗	✗	✓

HCM and RPC indicate harmonic current mitigation and reactive power compensation. # indicates RPC only

utilization and PQ, even when the battery is unavailable for V2G operations.

V2G operation supports the grid by providing active power support. Several studies demonstrate how effectively V2G operations can be managed to maintain a better voltage profile in the distribution network [10]. Earlier work focused on traditional V2G operation, which could only support the grid through API [9], [11]. The interface is redundant when an EV is unavailable. Authors in [12] have investigated the V2G operation involving reactive power compensation. However, harmonic current mitigation with the V2G interface has not been explored. Control of V2G for SC with Lyapunov function is reported by Çelik [13]. However, SC with multi-functional control involving simultaneous API and SC has not been explored.

[14]–[15] have presented a V2G interface with simultaneous API and SC. However, with SC, the VA rating of the interface may be exceeded, leading to operational constraints. Thus, an advanced M-V2G interface is needed to dynamically allocate VA capacity between API and SC while preventing overloading. Furthermore, the impact of different operating modes on PQ enhancement and system utilization remains underexplored in existing studies. The operating modes reported for V2G interfaces in various references are given in Table I. When the V2G interface supplies only active power to the load, the %THD of the supply current tends to increase [16].

For the implementation of SC, estimation of the FAC of load current is mandatorily needed. FACE based on generalized integrators, second-order filters, self-tuning filters, etc., are reported in the literature [7], [17]–[19]. These methods extract the input signal's fundamental component using second or higher-order transfer functions. While effective in isolating the fundamental component, these methods inherently exhibit slower dynamic responses due to the filtering stages involved. The transient response of such systems is further limited by the need for sufficient filtering to ensure accuracy. Moreover, these methods require precise tuning of multiple control parameters, which adds to the complexity. The computational burden of these techniques also poses challenges for real-time applications, especially when higher-order or multiple filtering stages are involved, requiring additional processing resources.

Least mean square (LMS) based FAC extraction techniques are also widely reported in the literature [17], [20]–[21]. LMS algorithms employ adaptive filtering structures, providing flexibility in harmonic order selection. However, LMS-based techniques require intensive computational resources and their dynamic and steady-state performance highly depends on the learning rate, μ. A higher μ leads to a faster dynamic response but introduces oscillations in steady-state conditions [22]–[23]. Conversely, a lower μ ensures accurate estimation at the cost of sluggish dynamic response [22]–[23]. LMS algorithms with variable learning rates (VLR), as reported in [24]–[27], mitigate this issue but increase the computational burden. Additionally, improper selection of μ may lead to instability [26]–[27]. This factor limits the practical usability of LMS for high-speed FACE in M-V2G applications.

[28]–[29] have explored artificial neural network (ANN)-based techniques for FAC extraction. ANN-based approaches require pre-training on large datasets corresponding to load profiles. However, their accuracy is compromised when the operating conditions deviate from the training dataset [29]. Furthermore, ANN implementations demand significant memory and processing power, making them less viable for real-time V2G control. Their reliance on extensive pre-training also reduces adaptability in dynamic grid conditions.

[2] and [30] introduced the moving window min-max (MWM) technique for FAC extraction. The MWM technique is simpler to implement, as it does not involve explicit filtering mechanisms and exhibits a faster dynamic response (approximately half a cycle). However, in intermediate calculations, the maximum and minimum values of the d-axis load current must be determined. Since no filtering is applied, accuracy is compromised when the sensed signals contain noise. In practical scenarios, this increases susceptibility to distortions, which can reduce the effectiveness of SC operation. Alternately, a computationally simple FACE with a faster dynamic response is required to facilitate seamless transitions between the operating modes of the M-V2G interface.

This paper presents an M-V2G interface with improved dynamic response for SC. As reported in [16], four operating modes of M-V2G, namely (A) API, (B) API and SC, (C) API and partial SC, and (D) SC, are considered in this paper. The improved dynamic response for SC is obtained with the proposed FACE unit. The proposed FACE is simpler to implement and provides an accurate estimation of FAC. The key idea behind the proposed algorithm is that for a signal containing dc and ac quantity, the dc quantity can be determined by sampling

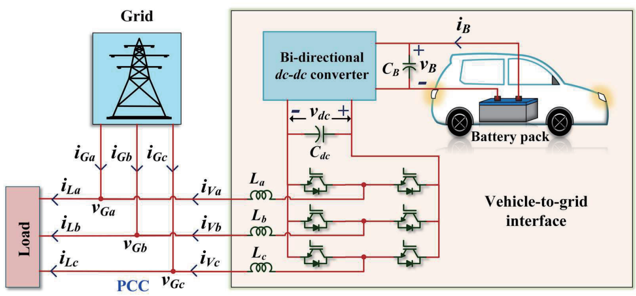

Fig. 1. Power circuit of M-V2G interface.

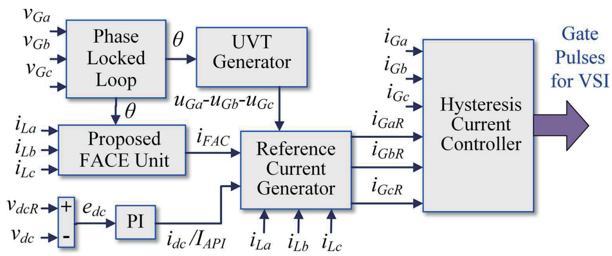

Fig. 2. Control circuit of M-V2G interface.

the signal at the peak of its derivate. This idea can be implemented for FAC extraction using d-axis load current, wherein the signal comprises both ac and dc quantities. The dc quantity represents the FAC of load current. The proposed FACE unit samples the d-axis load current, i_{Ld}, at the absolute peak value of $\mathrm{d}i_{Ld}/\mathrm{d}t$. Before this, i_{Ld} has been processed through cascaded band-stop filters (CBSFs). This filtering stage is required to eliminate higher-order harmonics so that only the lowest-order harmonic is present. The dynamic response of a second-order band-stop filter is faster when tuned to attenuate higher-order harmonics at their respective center frequencies than when set for the fundamental frequency. Hence, the overall dynamic response is not significantly impacted by the involvement of a cascaded band-stop filtering stage. Further, the obtained signal at the output of CBSFs is sampled at the absolute peak of its derivative. This sampled value represents the FAC of load current, i_{FAC}, which should be drawn from the grid to ensure SC. The mathematical basis of the proposed FACE is discussed in detail in further sections. Further frequency and time domain analysis are provided to validate fast dynamic response and accuracy for FAC extraction. The FACE method is computationally efficient, ensuring fast dynamic response and ripple-free steady-state operation. Unlike LMS-based approaches, it does not require iterative adaptation or learning rate tuning. Compared to ANN-based techniques, it eliminates the dependency on pre-trained models, making it more suitable for real-time operation. Further, the performance analysis of the M-V2G interface, based on the experimental studies, with the proposed FACE unit under four modes reveals its feasibility and practicability. With the merits of accurate and fast FAC extraction, computational simplicity, and ease of implementation, the FACE unit stands out as a key contribution. Furthermore, the proposed M-V2G control strategy ensures that even when API is not feasible due to battery unavailability, the voltage source inverter (VSI) can still be utilized for SC, improving overall system efficiency. This multi-functional operation enhances PQ at the point of common coupling (PCC) and maximizes the utilization of the V2G interface.

To summarize, the key contributions of this work are: (i) M-V2G operation enabling increased VA utilization, even in the absence of a battery for API operation, (ii) a novel FACE algorithm with fast dynamic response for the implementation of SC using the M-V2G interface, (iii) frequency response analysis and step response analysis conducted to validate effective filtering and rapid dynamic response, and (iv) experimental validation of the four operating modes, demonstrating the feasibility and practical implementation of the proposed FACE-based control for the V2G interface.

II. Operation of Multi-Functional V2G Interface

The EV charger employs ac-dc and dc-dc converters to charge EV batteries from the grid. The charging process of EV batteries from the grid refers to G2V operation. EVs can provide auxiliary services to the grid, such as grid support through API. Such operation of an EV charger wherein power flows from the EV battery to the grid is referred to as the V2G operation. For EVs to facilitate V2G operations, the employed converters in the interface should be bidirectional. Fig. 1 shows the power circuit of the M-V2G interface, comprising a battery interfaced with the grid through a bidirectional dc-dc converter and VSI. VSI is interfaced with the grid through coupling inductors, L_a-L_b-L_c. In Fig. 1, v_{Ga}-v_{Gb}-v_{Gc} are grid voltages at the PCC with frequency ω and phase angle θ, i_{Ga}-i_{Gb}-i_{Gc} are grid currents, i_{La}-i_{Lb}-i_{Lc} are load currents, i_{Va}-i_{Vb}-i_{Vc} are currents supplied by the V2G interface, C_{dc} is the dc-link capacitor, v_{dc} is the dc-link voltage, and v_{B}-i_{B} are battery voltage and battery current. For the traditional V2G operation, EVs are required. The V2G interface is redundant in case (i) batteries are not available for the V2G operations and (ii) the state of charge (SOC) of the battery is not adequate. Also, in case the available battery has a lower capacity than the rating of the V2G interface, the interface will not be utilized to its maximum rating. This work proposes multi-functional control of the V2G interface with a fast dynamic response for SC.

The block diagram depiction of multi-functional control of the V2G interface is mentioned in Fig. 2. The phase-locked loop (PLL) algorithm processes v_{Ga}-v_{Gb}-v_{Gc} and computes phase angle, θ. Based on estimated θ, unit vector templates (UVTs), u_{Ga}-u_{Gb}-u_{Gc}, are computed. The proposed FACE unit utilizes i_{La}-i_{Lb}-i_{Lc} and θ for the computation of FAC of load current denoted as i_{FAC}. With the two-stage system, as shown in Fig. 1, the dc-dc converter will feed power at the dc-link for API. For G2V operation, ac-dc conversion is required. It is accomplished by regulating the dc-link voltage. When dc-dc draws power from dc-link for charging the battery pack, v_{dc} starts decreasing. On the contrary, when the dc-dc converter injects power into the dc-link from the battery pack, v_{dc} starts rising. The dc-link voltage control loop regulates v_{dc} by drawing power from the grid when required for the battery charging and injecting

TABLE II
OPERATION AND REFERENCE CURRENT FOR EACH MODE

Current	Mode	Operation		Reference Current for V2G Interface $i_{VxR}(t)$	
		API	SC		
$i_{VxR}(t)$	A	✓	✗	$i_{VxR}(t) = I_{API}\ u_{Gx}(t)$	(1)
	B	✓	✓	$i_{VxR}(t) = I_{API}\ u_{Gx}(t) + i_{SCx}(t)$	(2)
	C	✓	Δ	$i_{VxR}(t) = I_{API}\, u_{Gx}(t) + K\, i_{SCx}(t)$ $K{=}(I_{RM} - I_{API}) / max\{z_a, z_b, z_c\}$	(3) (4)
	D	✗	✓	$i_{VxR}(t) = i_{SCx}(t)$	(5)
$i_{SCx}(t)$	B, C, D	-	-	$i_{SCx}(t) = i_{Lx}(t) - i_{FAC}(t)\, u_{Gx}(t)$	(6)
$i_{GxR}(t)$	A, B, C, D	-	-	$i_{GxR}(t) = i_{Lx}(t) - i_{VxR}(t)$	(7)

✓ - ✗ - Δ correspondingly indicates that the functionality can be, cannot be, or is partially implemented.

power to the grid during API operation. v_{dc} is compared with a reference voltage, v_{dcR} and the resulting dc-link voltage error, e_{dc}, is processed by the proportional-integral (PI) controller for computing the peak value of active current to be injected into the grid for regulation of v_{dc}, denoted as i_{dc}. It is to be noted that i_{dc} represents active power consumed by the VSI on account of losses and active power demanded or injected by the dc-dc converter. Neglecting the losses compared to the active power being exchanged at the dc-link, i_{dcR} can be represented as I_{API}. I_{API} represented as the peak value of FAC of injected currents at PCC. The corresponding product of I_{API} and u_{Ga}-u_{Gb}-u_{Gc}, denoted as i_{dcRa}-i_{dcRb}-i_{dcRc}, represents the instantaneous values of active current to be injected into the grid for regulation of v_{dc}. The dc-link voltage control loop facilitates ac-dc conversion during battery charging and dc-ac conversion during API operation. Based on the active operating mode, I_{API}, i_{La}-i_{Lb}-i_{Lc}, and i_{FAC}, reference grid currents, denoted as i_{GaR}-i_{GbR}-i_{GcR}, are determined. Based on i_{GaR}-i_{GbR}-i_{GcR} and i_{Ga}-i_{Gb}-i_{Gc}, hysteresis current controller generates gate pulses for the VSI of M-V2G interface.

The multi-functional operation of the V2G interface refers to the implementation of SC alongside traditional API operation. The power interface between the grid and the vehicle is designed based on the charging requirement of the battery. However, when implementing V2G operation, the batteries may not be discharged at full capacity, or sometimes lower capacity batteries are available for V2G operation. In such a scenario, the power interface may not be operated at its rated capacity. To increase the utilization of the V2G interface, SC can be implemented for the other loads at the station premise alongside API. This not only increases VA utilization of the V2G interface but also helps in improving the PQ. The four operating modes of the proposed M-V2G interface are (A) API only, (B) API and SC, (C) API with partial SC, and (D) SC only. For each mode, Table II shows the functionality, reference current for the V2G interface, $i_{VxR}(t)$, currents for SC, $i_{SCx}(t)$, and reference grid currents, $i_{GxR}(t)$, through (1)-(7). Mode-A implements traditional V2G with API only. Hence, $i_{VxR}(t)$ is the product of reference API, I_{API}, and respective UVT, $u_{Gx}(t)$, which are obtained using PLL. x in subscript denotes phase a, b, or c.

Although the traditional API operation assists the grid in supplying active power to the load, it does not resolve the harmonic current injection issue due to other nonlinear loads at the station. To increase VA utilization of the V2G interface and improve the PQ at the PCC, Mode-B implements M-V2G operation with concurrent API and SC. $i_{SCx}(t)$ is computed as per (6). $i_{VxR}(t)$ is the sum of $i_{SCx}(t)$ and $[I_{API}u_{Gx}(t)]$. It is to be noted that the V2G interface is designed based on the charging requirements. In case of an increase in load at the PCC, the V2G interface might run at overload. When the peak current capacity of VSI, I_{RM}, is exceeded, Mode-C is used, where $i_{VxR}(t)$ can be computed as per (3) and $i_{SCx}(t)$ is scaled by the scaling factor K. K is defined in (4), where z_x is the absolute peak of $i_{SCx}(t)$ computed over a cycle. API in Mode-C is as per I_{API}, and only SC is scaled. A similar approach is reported in [16] and [31] for the multi-functional control of battery and solar photovoltaic systems. Mode-D is activated when no battery is available. Only SC takes place in Mode-D, and the V2G interface only provides $i_{SCx}(t)$. The Mode-D operation of the V2G interface increases the utilization of the V2G interface by implementing SC even when the batteries are not available for the API operation. Thus, Modes A, B, and C require the grid to partially support the APDL. Modes B and D fully provide the required SC, whereas Mode-C performs partial SC as per the available VA ratings. In Modes A and C, the grid provides for the current harmonics and RPDL fully and partially, respectively. In Modes B, C, and D, the FACE unit needs to compute i_{FAC} for implementing SC.

Mode A to C can be implemented when the battery is fully charged. API and API with full or partial shunt compensation can be implemented with the battery fully charged. With API, the battery gets discharged. Even Mode-D can be activated in such a scenario, provided API is not to be carried out. Ideally, the battery will not discharge with Mode-D, and the V2G interface will be utilized for SC. On the other hand, when the battery is fully depleted, Mode A to C cannot be activated. In such a scenario, only Mode-D can be activated. No API will take place. However, SC will be carried out to enhance PQ and improve the overall utilization of the charging infrastructure. For Modes B, C, and D, computation of i_{FAC} is required to perform SC.

TABLE III
PSEUDO-CODE FOR THE PROPOSED FACE

Operation	Mathematical Operation	
Initialize sampling instant n as 1		
Sample i_{La} - i_{Lb} - i_{Lc} and obtain $u_{Ga}(n)$ - $u_{Gb}(n)$ - $u_{Gc}(n)$ from the PLL.		
Compute i_{Ld}	$i_{Ld}(n) = (2/3)\times\sum_{x=a,b,c} i_{Lx}(n)\, u_x(n)$	(8)
	$=i_{FAC}(n)+\sum_{l=2,6,12,18,24} M_l(n)\sin[l\theta(n)+\varphi_l]$	(9)
Compute i_y	For a balanced system, $i_y(n) = i_{FAC}(n) + M_6(n)\sin[6\theta(n)+\varphi_6]$	(10)
	For an unbalanced system, $i_y(n) = i_{FAC}(n) + \sum_{l=2,6} M_l(n)\sin(l\theta(n)+\varphi_l)$	(11)
Compute $\lvert pi_y \rvert$	For a balanced system, $\lvert pi_y(n)\rvert = \lvert 6M_6(n)\cos[6\theta(n)+\varphi_6]\rvert$	(12)
	For an unbalanced system, $\lvert pi_y(n)\rvert = \lvert \sum_{l=2,6} lM_6(n)\cos[l\theta(n)+\varphi_l]\rvert$	(13)
Update i_{FAC}	$J(n) = \lvert pi_y(n)\rvert$	(14)
	Condition: $J(n-1) \geqslant J(n)$ & $J(n-1) \geqslant J(n-2)$	(15)
	$i_{FAC}(n) = i_y(n-1)$	(16)
Repeat the process with $n = n + 1$.		

III. PROPOSED FACE UNIT

The d-axis load current for non-linear loads comprises a dc and several ac components. For a signal comprising an ac and a dc quantity, the sampling of the signal at the absolute peak of its derivative represents the dc component. This logic does not right away apply to the extraction of FAC as multiple ac signals are present in the d-axis load current. CBSFs processes the d-axis load current to remove all ac components other than the lowest order harmonic in order to get around the problem before sampling or computing the derivative. The FAC of load current can now be computed by sampling the obtained signal at the peak of its derivative.

Table III shows the procedure for the proposed FACE unit, with p as the differential operator. Based on the input samples, the d-axis load current, i_{Ld}, is determined as per (8). To remove high-frequency noise, i_{Ld} is low pass filtered with a cut-off frequency, δ, of 1000 Hz. As shown in (9), where l is the order of harmonic and φ_l is the phase-shift angle of l^{th} harmonic, i_{Ld} comprises of i_{FAC} as the dc component and multiple ac components representing the harmonics. If there was only one ac component in i_{Ld}, then i_{FAC} could be determined as the sample of i_{Ld} at the absolute peak of its derivative. To apply this idea, the 12th, 18th, and 24th harmonic present in i_{Ld} are filtered out by processing it through CBSF having a center frequency, δ_b, of 12ω, 18ω, and 24ω, respectively. The step response analysis of the band stop filter (BSF) reveals a faster dynamic response with higher δ_b. As shown by (10)–(11), in addition, i_{FAC} to the output of CBSF, i_y, comprises the 6th harmonic and 2nd plus 6th harmonic for balanced and unbalanced currents, respectively. Here, M_l is the peak magnitude of the lth harmonic.

The proposed idea necessitates the determination of the

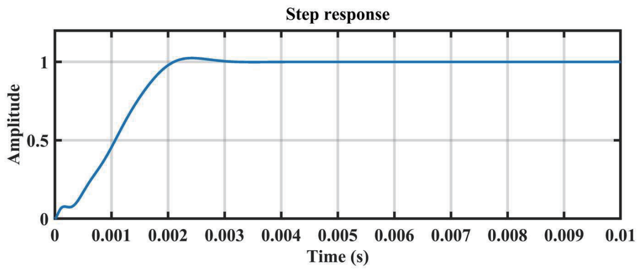

Fig. 3. Step response of CBSF implemented for balanced loading conditions.

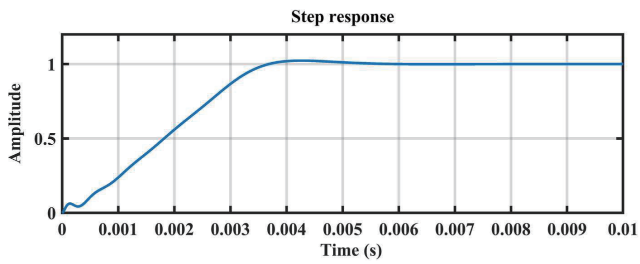

Fig. 4. Step response of CBSF implemented for unbalanced loading conditions.

peak of $\lvert pi_y \rvert$, which is given by (12)–(13) for balanced and unbalanced cases. With J defined by (14), when the conditions specified in (15) are satisfied, i_{FAC} is updated as per (16). For the balanced case, $i_{FAC}(n) = i_y(n-1)$, which can be estimated by sampling i_y at the peak of $\lvert pi_y(n)\rvert$. At the peak of $\lvert pi_y(n)\rvert$, $p^2 i_y(n)$, given by (17), is equated to zero, and the roots (i.e. θ) are determined. Since $M_6 > 0$, $p^2 i_y(n) = 0$ holds true when $\sin[(6\theta(n)+\varphi_6] = 0$, which leads to $[6\theta(n)+\varphi_6] = \pi$ or 2π. At θ, given by (18), $i_y(n) = i_{FAC}(n)$. This proves the proposed idea.

For an unbalanced case, as two ac quantities present in i_y. Hence, i_{FAC} cannot be estimated by sampling i_y at the peak of $\lvert pi_y \rvert$. The use of BSF to eliminate the 2nd harmonic can resolve the issue, but the response time for BSF is higher for the 2nd order harmonic. Alternately, if 6th harmonic is eliminated using BSF, then similar approach as given by (14)–(16) is followed. T_R, the maximum time for computing the new value of i_{FAC} upon change in load, is given by (19), where t_L-t_{CBSF}-t_h correspondingly indicate the response time of LPF, response time of BSFs involved, and maximum time between the instants of load change and next peak of $\lvert pi_y(n)\rvert$. The step response for CBSF under balanced and unbalanced load conditions are shown in Figs. 3 and 4, respectively. Based on the step response analysis using MATLAB's stepinfo function, T_R for balanced and unbalanced cases is determined as 4.3 ms and 9.6 ms, respectively. Hence, for instant change in load, the new value of FAC will be estimated within 9.6 ms. Further, bode plots for CBSF utilized for balanced and unbalanced conditions are shown in Figs. 5 and 6, respectively. It is to be observed from bode plots that the higher order harmonics are attenuated as magnitude/attenuation at their frequencies is very close to zero.

$$p^2 i_y(n) = -36M_6(n)\sin[6\theta(n)+\varphi_6] \tag{17}$$

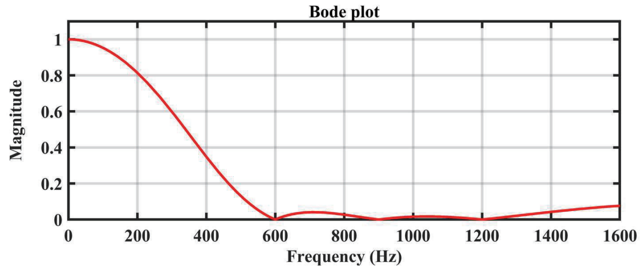

Fig. 5. Bode plot of CBSF implemented for balanced loading conditions.

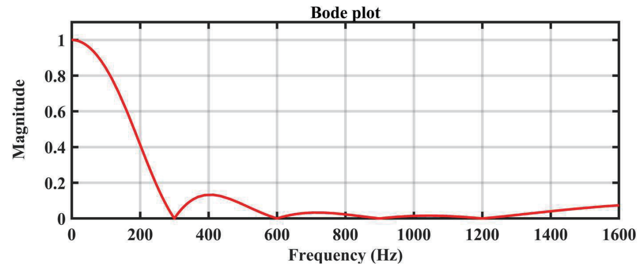

Fig. 6. Bode plot of CBSF implemented for unbalanced loading conditions.

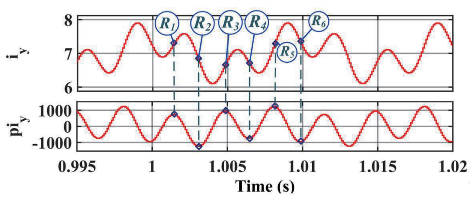

	Time	i_y
R_1	1.0014	7.29364
R_2	1.0031	6.71699
R_3	1.0048	6.65082
R_4	1.0064	6.70822
R_5	1.0081	7.28529
R_6	1.0098	7.35129
Average		7.001

Fig. 7. i_y and pi_y for unbalanced loading.

$$\theta = [(\pi - \varphi_6)/6] \text{ or } [(2\pi - \varphi_6)/6] \tag{18}$$

$$T_{\mathrm{R}} = t_{\mathrm{L}} + t_{\mathrm{CBSF}} + t_h \tag{19}$$

Another approach is proposed for the estimation of i_{FAC} under unbalanced conditions. For the unbalanced case, as per (11) and (13), there would be two ac quantities present in $i_y(n)$ and $|pi_y(n)|$. Now, i_{FAC} cannot be estimated by sampling i_y at the peak of $|pi_y|$. As presented earlier, the use of BSF to eliminate either the 2$^{\mathrm{nd}}$ or 6$^{\mathrm{th}}$ harmonic can resolve the issue. The elimination of the 2$^{\mathrm{nd}}$ harmonic would incur increased response time compared to proceeding with the elimination of the 6$^{\mathrm{th}}$ harmonic component. However, one more filtering stage would be required. Another approach is presented wherein an additional filter for removing either the 2$^{\mathrm{nd}}$ or 6$^{\mathrm{th}}$ harmonic is not required. For unbalanced load currents, i_y and pi_y are shown in Fig. 7. i_y sampled at the peak of $|pi_y|$ over a 10 ms duration (i.e. time period of 2$^{\mathrm{nd}}$ harmonic) are given by R_1-R_6. These six consecutive samples are stored in an array based on first-in-last-out, and as per (20), the average of six samples represents i_{FAC} as given in (21). As shown in Fig. 7, the average of R_1-R_6 is 7.001 A, which is equal to i_{FAC}. This approach of computing i_{FAC} based on averaging the values of i_y sampled at the peak of $|pi_y|$ over a 10 ms duration has a larger response time than the previous approach. Further, FAC estimated with the proposed FACE unit will be utilized by the overall control algorithm to implement various operating modes of the M-V2G interface. The proposed FACE offers accurate estimation and a fast dynamic response and is easier to implement.

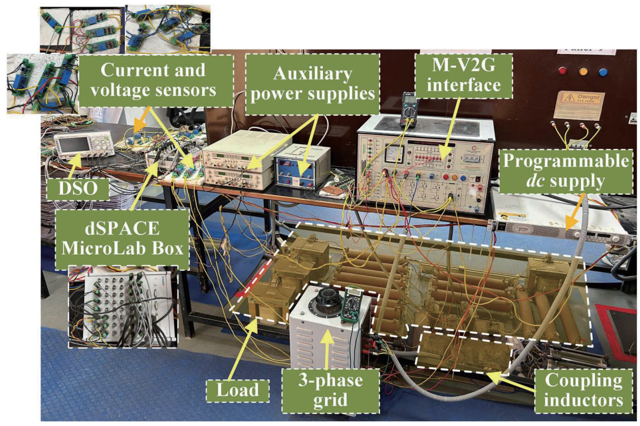

Fig. 8. Experimental prototype model of M-V2G controlled with the proposed FACE.

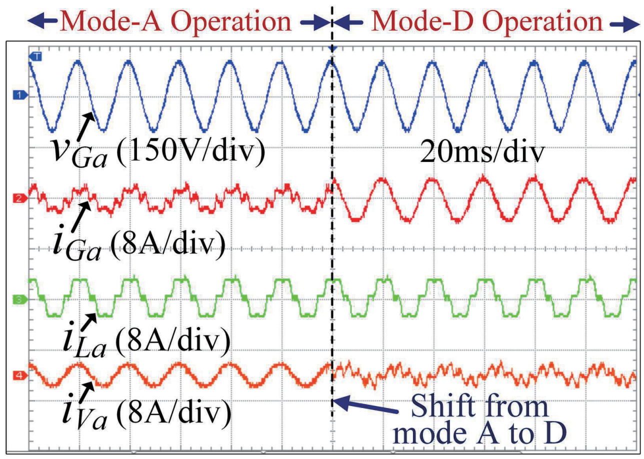

Fig. 9. Performance analysis of M-V2G interface with the proposed FACE. v_{Ga}-i_{Ga}-i_{La}-i_{va} for mode transition from Mode A-D.

$$\text{For } j = 5{:}1,\ \mathrm{A}(j+1) = \mathrm{A}(j)\ \&\ A(1) = i_y(n) \tag{20}$$

$$i_{\mathrm{FAC}} = \frac{1}{6}\sum_{k=1}^{6} A(k) \tag{21}$$

IV. Results and Discussions

Experimental studies are performed to validate the performance of the M-V2G interface controlled with the proposed FACE unit. The experimental setup is shown in Fig. 8. The V2G interface comprises a 3-phase grid-tied VSI employing IGBTs SKM100GB12T4. v_{Gx} is 70.7 V, and nominal grid frequency is 50 Hz. The value of L_{x} is 10 mH. The value of C_{dc} is 1500 μF. The control algorithm, comprising overall multi-functional control comprising the proposed FACE unit, is

TABLE IV
LIST OF PARAMETERS USED IN EXPERIMENTAL STUDY

Parameter	Value
Supply	3-phase, 122.47 V ac voltage
Nominal supply frequency	50 Hz
IGBT part no.	SKM100GB12T4
L_a - L_b - L_c	10 mH
C_{dc}	1500 μH
Controller	dSPACE MicroLab Box 1202
Voltage sensors	LV25-P/SP2
Current sensors	LA55-P/SP1

Load Configurations

	Load (Ω)						Load Parameters (Ω)
	I	II	III	IV	V	VI	
R_{DBR}	50	25	50	50	25	25	Impedance/phase of the 3-phase R-L load
	--	--	Z_1	Z_1	Z_1	Z_1	$Z_1 = 50 + j\omega 0.2$
Z_{LIN}	--	--	Z_1	Z_1	Z_1	Z_1	$Z_2 = 32 + j\omega 0.03$
	--	--	Z_1	Z_2	Z_1	Z_2	

TABLE V
MEASURED PEAK VALUES AND %THD OF i_{Ga}-i_{La}-i_{Va} FOR THE FOUR OPERATING MODES

Mode	Peak Value			%THD		
	i_{Ga}	i_{La}	i_{Va}	i_{Ga}	i_{La}	i_{Va}
Mode-A	2.1	3.1	2.0	38.0	19.6	4.6
Mode-B	3.2	4.3	3.0	4.0	15.0	30.0
Mode-C	5.8	6.9	3.4	6.7	13.3	25.0
Mode-D	3.5	3.1	2.3	3.5	20.3	61.0

implemented in dSPACE MicroLab Box 1202. For feedback, LV25-P/SP2 voltage sensors and LA55-P/SP1 current sensors are used. Load comprises of parallel connection of 3-phase uncontrolled rectifier with a load resistance of R_{DBR} and 3-phase RL load. The list of parameters used in experimental studies are given in Table IV. Programmable dc power supply emulates EV battery and bi-directional dc-dc converter.

Figs. 9 and 10 show the performance analysis of the M-V2G interface with the proposed FACE for phase-a. Figs. 9 and 10 exhibit performance during transitions from Modes A-D and B-C, respectively. The peak magnitudes (PMs) and THD of i_{Ga}-i_{La}-i_{Va} are indicated in Table V for each mode. With Load-I, for Modes A and D, i_{La} is non-sinusoidal with PM and THD of 3.1-3.1 A and 19.6%-20.3%. In Fig. 9, during Mode-A, the M-V2G interface performs API with I_{API} of 2.0 A. Hence, i_{Va} is sinusoidal with %THD<5. i_{Ga} caters to RPDL, current harmonics of load, and the remaining APDL. It is now equal to (i_{La}-i_{Va}), and it provides RPDL fully and APDL partially. Hence, the THD of i_{Ga} exceeds 5%. Now, if the battery is unavailable, the system shifts to Mode-D and M-V2G interface performs SC as per the proposed FACE unit to deliver i_{SCa}. Hence, i_{Va} is highly distorted. But, i_{Ga} is sinusoidal and in-phase with v_{Ga} as it needs to cater to APDL only. Thus, with Mode-D, the system is not redundant when the battery is unavailable and performs PQ enhancement.

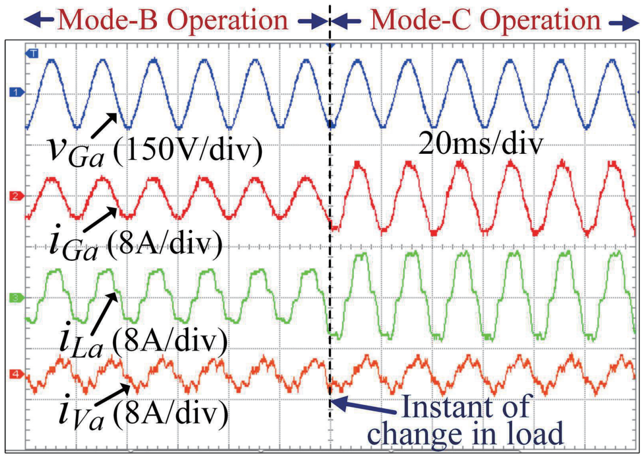

Fig. 10. Performance analysis of M-V2G interface with the proposed FACE. v_{Ga}-i_{Ga}-i_{La}-i_{va} for mode transition from Mode B-C.

TABLE VI
POWER ANALYSIS FOR THE FOUR OPERATING MODES

Mode	Load	Grid		Load		M-V2G Interface	
		P_G (W)	Q_G (VAr)	P_L (W)	Q_L (VAr)	P_V (W)	Q_V (VAr)
A	I	214	136	472	147	258	11
B	III	467	−2	567	285	100	287
C	V	812	179	912	508	100	329
D	I	505	0	465	146	−40	146

Fig. 10 shows the M-V2G operation for Mode B-C. In Mode-B, the M-V2G interface performs API to partially meet the APDL and SC. Load-III is present in Mode-B. As a result of SC implemented by the M-V2G interface, i_{Va} is non sinusoidal and i_{Ga} is sinusoidal with %THD<5. Mode-C is initiated with Load-V and I_{RM} - I_{API} as 4.0-1.0A, and K = 0.645. K<1 indicates partial SC. Hence, 64.5% of i_{SCa} is supplied by the M-V2G interface and the remaining is catered by the grid. With partial SC as per I_{RM} limit, M-V2G interface ensures that the THD of i_{Ga} is less than that of i_{La}. The proposed FACE unit facilitates seamless operation and transitions between M-V2G functionalities. Such M-V2G operation increases VA utilization while adhering to VA ratings.

The active and reactive power supplied by the grid, P_G - Q_G, supplied by the M-V2G interface, P_V - Q_V, and consumed by the load, P_L - Q_L, are given in Table VI. In Mode-A, P_V partially meets the APDL and does not perform SC. Hence, the grid caters to the remaining APDL. As SC is absent, $Q_L = Q_G$. Also, the harmonic currents are fed from the grid. In Mode-B, as the M-V2G interface performs SC and API, $Q_V = Q_L$, $Q_G = 0$, and

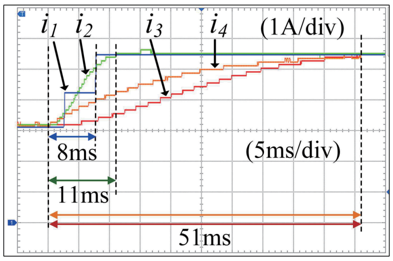

Fig. 11. Dynamic response analysis for balanced load.

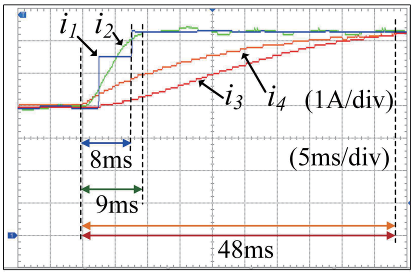

Fig. 12. Dynamic response analysis for unbalanced load (Load-IV to Load-VI).

APDL is met by the grid and M-V2G interface. Hence, $P_L = P_G + P_V$. In Mode-C, partial SC is implemented by the interface to avoid its overloading, $Q_L = Q_G + Q_V$. Also, the M-V2G interface now partially caters to APDL. With the unavailability of a battery, the operation shifts to Mode-D, wherein SC is performed by the V2G interface. Hence, $Q_G = 0$ and $Q_L = Q_V$. Now, as APDL is met by the grid, $P_L = P_G$.

Figs. 11 and 12 show the steady-state and dynamic response for i_1 - i_4 for balanced and unbalanced loads with time to reach the new steady state indicated individually. i_1 - i_4 respectively denote the FAC computed with the proposed method, synchronous reference frame theory (SRFT) with filter cut-off frequency, δ, of 50 Hz, SRFT with $\delta = 10$ Hz, and LMS algorithm with $\mu = 0.01$, reported in [20]. The comparison of the FAC extraction with these four methods is given in Table VII, while the estimated values are mentioned in Table VIII. With the change from Load-I to Load-II, i_1 has the fastest dynamic response, and i_3 has a sluggish response. With larger δ, i_2 has a faster response as compared to i_3. However, as observed from Fig. 12, with the unbalanced loading (Load IV to VI), the higher δ cannot fully attenuate the 2nd harmonics, and hence ripples are observed in the steady state. However, this is not the case with the proposed method; no ripples are observed in the steady-state, even for unbalanced loading. LMS algorithm exhibits a slower dynamic response for the given μ and considered loads. The optimal selection of a variable μ can improve the response, but the computational complexity will significantly increase. The experimental studies validate the fast, dynamic and accurate steady-state response of the proposed FACE.

TABLE VII
COMPARISON OF FACE BASED ON EXPERIMENTAL STUDIES

FACE	Load	SRF δ=50 Hz	SRF δ=10 Hz	ADALINE - LMS	Proposed
Ripples	Balanced	Less	Not observed	Not observed	Not observed
	Unbalanced	High	Not observed	Not observed	Not observed
Transition Time (ms)	Balanced	11	51	51	8
	Unbalanced	9	48	48	8

TABLE VIII
ESTIMATED VALUES WITH DIFFERENT FAC EXTRACTION TECHNIQUES

Load	Average value of FAC estimated with the proposed SRFT with δ=50 Hz, SRFT with δ=10 Hz, and LMS algorithm with μ=0.01 for Loads I, II, IV and VI (A)			
	i_1	i_2	i_3	i_4
I	3.0	3.0	3.0	3.05
II	5.3	5.3	5.3	5.4
IV	3.9	3.9	3.9	3.9
VI	6.2	6.2	6.2	6.3

V. CONCLUSION

This paper proposes an M-V2G interface with a new FACE unit for improved dynamic response for SC. The reported M-V2G operation performs (A) API only, (B) API and SC, (C) API and partial SC, and (D) SC only. FACE is mandatorily needed for Modes B, C, and D. A new FACE unit is proposed, which offers the benefits of computation simplicity, ease of implementation, fast dynamic response, and ripple-free steady-state response. The merits of the proposed scheme are evident from the presented comparative analysis. Also, the fast dynamic response offered by the proposed extraction scheme results in a seamless transition among the various operating modes. If a signal comprising of an ac and a dc component is sampled at the absolute peak of its derivative, then the sample value is the dc component. With non-linear loads, the d-axis load current comprises a dc and several ac components. Hence, this logic is not directly applicable to FAC extraction. To circumvent the issue, before sampling or computing the derivative, the d-axis load current is processed through CBSF to remove all ac components except the lowest-order harmonic. Now, the value sampled as per the concept mentioned earlier represents the FAC of load current. The excellent harmonic attenuation capability and fast dynamic response of the CBSF are evident from the presented frequency and step response analysis. Mathematical derivations for the FACE and steps for controlling the M-V2G interface for each mode are discussed in detail. Further, the performance of M-V2G has been experimentally validated for the four operating modes. Such multi-functional operation can result in PQ enhancement through SC, support the grid through API, improve the VA utilization of the M-V2G interface, and facilitate the use of the interface even when the battery is unavailable.

References

[1] S. S. Letha, M. H. J. Bollen, and T. Busatto, and Á. Espín-Delgado, "Power quality issues of electro-mobility on distribution network—An overview," in *Energies*, vol. 16, no. 13, Jun. 2023.

[2] A. J. Patel and A.V Sant, "Power quality enhancement for charging station with moving window min-max algorithm-based shunt active power filter," in *Energy Reports*, vol. 8, pp. 86–91, Oct. 2022.

[3] D. Çelik and M. E. Meral, "A coordinated virtual impedance control scheme for three-phase four-leg inverters of an electric vehicle to grid (V2G)," in *Energy*, vol. 246, May 2022.

[4] M. R. Khalid, M. S. Alam, A. Sarwar, and M. J. Asghar, "A Comprehensive review on electric vehicles charging infrastructures and their impacts on power-quality of the utility grid," in *ETransportation*, vol. 1, Aug. 2019.

[5] S. Behera, N V. R. Naik, A. K. Panda, and S. K. Behera, "A dual control strategy for improved power quality in grid-tied off-board bidirectional electric vehicle charger," in *Electric Power Systems Research*, vol. 236, Nov. 2024.

[6] R. K. Lenka, A. K. Panda, and L. Senapati, "Grid integrated multifunctional EV charging infrastructure with improved power quality," in *Journal of Energy Storage*, vol. 76, Jan. 2024.

[7] A. J. Patel and A. V. Sant, "EV charging station with cascaded low-pass filtering scheme-based control of unified power quality conditioner," in *Clean Energy*, vol. 6, no. 5, pp. 738–761, Oct. 2022.

[8] C. Balasundar, C. K. Sundarabalan, J. Sharma, N. S. Srinath, and J. M. Guerrero, "Design of power quality enhanced sustainable bidirectional electric vehicle charging station in the distribution grid," in *Sustainable Cities and Society*, vol. 74, Nov. 2021.

[9] Y. Wang, J. -W. Yang, W. -J. Kim, T. -H. Kwon, T. Lee, and S. -J. Park, "Second harmonic current suppression and dynamic response improvement for V2G system," in *IEEE Transactions on Power Electronics*, vol. 38, no. 8, pp. 9566–9580, Aug. 2023.

[10] S. Das, P. Thakur, A. K. Singh, and S. N. Singh, "Optimal management of vehicle-to-grid and grid-to-vehicle strategies for load profile improvement in the distribution system," in *Journal of Energy Storage*, vol. 49, May 2022.

[11] A. Zabetian-Hosseini, G. Joós, and B. Boulet, "Control design for effective usage of electric vehicles in V2G-enabled DC charging stations," in *IEEE Transactions on Power Delivery*, vol. 38, no. 6, pp. 4335–4346, Dec. 2023.

[12] A. A. Ghani, V. K. Ramachandaramurthy, and J. Y. Yong, "Design of a master power factor controller for an industrial plant with solar photovoltaic and electric vehicle chargers," in *Electrical Engineering*, vol. 104, no. 1, pp. 13–25, Feb. 2022.

[13] D. Çelik, "Lyapunov based harmonic compensation and charging with three phase shunt active power filter in electrical vehicle applications," in *International Journal of Electrical Power & Energy Systems*, vol. 136, Mar. 2022.

[14] K. Srivastava, S. Kumar, and R. Maurya, "A robust BCNMCC based variance smoothing approach for SPV based grid integrated EV battery charging system," in *Journal of Energy Storage*, vol. 72, Nov. 2023.

[15] R. K. Lenka, A. K. Panda, R. Patel, and J. M. Guerrero, "PV integrated multifunctional off-board EV charger with improved grid power quality," in *IEEE Transactions on Industry Applications*, vol. 58, no. 5, pp. 5520–5532, Sept.-Oct. 2022.

[16] A. J. Patel and A. V. Sant, "A new fundamental active current extraction scheme for multifunctional control of V2G interface," in *Journal of Energy Storage*, vol. 86, May 2024.

[17] A. V. Sant, "Shunt active power filtering with reference current generation based on dual second order generalised integrator and LMS algorithm," in *Energy Reports*, vol. 8, pp. 886–893, Nov. 2022.

[18] S. Ahmed, G. Madjid, M. Youcef, and T. Hamza, "Real-time control of an active power filter under distorted voltage condition," in *International Journal of Power Electronics and Drive Systems*, vol. 2, no. 4, pp. 424–433, Dec. 2012.

[19] C. Singh, G. Kumar, H. Kumar, and A. Arora, "Power quality enhancement using adaptive notch filter in grid distribution system," in *2023 3rd International Conference on Intelligent Technologies (CONIT)*, Hubli, India, 2023, pp. 1–6.

[20] A. Kumar and P. Kumar, "Power quality improvement for grid-connected PV system based on distribution static compensator with fuzzy logic controller and UVT/ADALINE-based least mean square controller," in *Journal of Modern Power Systems and Clean Energy*, vol. 9, no. 6, pp. 1289–1299, Nov. 2021.

[21] S. K. Patel, S. R. Arya, and R. Maurya, "Optimal step LMS-based control algorithm for DSTATCOM in distribution system," in *Electric Power Components and Systems*, vol. 47, no. 8, pp. 675–691. Aug. 2019.

[22] Q. Niu and T. Chen, "A new variable step size LMS adaptive algorithm," in *2018 Chinese Control and Decision Conference (CCDC)*, Shenyang, China, 2018, pp. 1–4.

[23] N. Gupta, M. Morey, M. M. Garg, and A. Kumar, "An experimental investigation of variable-step-size affine projection sign based algorithm for power quality enhanced grid-interactive solar PV system," in *Electric Power Systems Research*, vol. 228, Mar. 2024.

[24] S. Roy, F. Chishti, B. Singh, and B. K. Panigrahi, "GNLMP control for solar PV-battery based microgrid with Ms-EPLL synchronization," in *IEEE Transactions on Industry Applications*, vol. 58, no. 5, pp. 6599–6611, Sept.-Oct. 2022.

[25] A. Parida and B. Subudhi, "A variable step size robust least mean logarithmic square-based control scheme for improved power quality of grid-interfaced PV system," in *IEEE Transactions on Smart Grid*, vol. 13, no. 3, pp. 2086–2093, May 2022.

[26] B. Singh, S. K. Dube, and S. R. Arya, "Hyperbolic tangent function-based least mean-square control algorithm for distribution static compensator," in *IET Generation, Transmission & Distribution*, vol. 8, no. 12, pp. 2102–2113, Dec. 2014.

[27] P. A. C. Lopes, "Analysis of the LMS and NLMS algorithms using the misalignment norm," in *Signal, Image and Video Processing*, vol. 17, pp. 3623–3628, May 2023.

[28] A. Bhattacharya and C. Chakraborty, "A shunt active power filter with enhanced performance using ANN-based predictive and adaptive controller," in *IEEE Transactions on Industrial Electronics*, vol. 58, no. 2, pp. 421–428, Feb. 2011.

[29] M. Qasim and V. Khadkikar, "Application of artificial neural networks for shunt active power filter control," in *IEEE Transactions on Industrial Informatics*, vol. 10, no. 3, pp. 1765–1774, Aug. 2014.

[30] A. J. Patel and A. V. Sant, "Moving window min-max algorithm-based control of UPQC at EV charging station," in *2023 IEEE 3rd International Conference on Smart Technologies for Power, Energy and Control (STPEC)*, Bhubaneswar, India, 2023, pp. 1–6.

[31] A. V. Sant, V. Khadkikar, W. Xiao, H. Zeineldin, and A. Al-Hinai, "Adaptive control of grid connected photovoltaic inverter for maximum VA utilization," in *IECON 2013-39th Annual Conference of the IEEE Industrial Electronics Society*, Vienna, Austria, 2013, pp. 388–393.

Arpitkumar J. Patel is currently pursuing a Ph.D. in Electrical Engineering at Pandit Deendayal Energy University, focusing on the multifunctional control of custom power devices for EV charging stations incorporating Solar PV systems. He holds an M.Tech in Electrical Engineering (Power Systems) from Pandit Deendayal Energy University, where he worked on the control of grid-tied inverters. He completed his B.E. in Electrical Engineering from Gujarat Technological University. His research interests include electric vehicle charging systems, power electronic converters, power quality, and control algorithms.

Amit V. Sant received Ph.D. degree in Power Electronics from the Indian Institute of Technology Delhi, New Delhi, India, in 2013. Presently, he is an Associate Professor in the Department of Electrical Engineering, School of Energy Technology, Pandit Deendayal Energy University (PDEU), Gandhinagar, Gujarat, India. Before joining PDEU, he was a Postdoctoral Research Researcher at the Masdar Institute of Science and Technology, Abu Dhabi, United Arab Emirates. His present research focuses on multilevel inverters, z-source inverters, high gain DC-DC converters, grid integration of renewables, charging infrastructure for electric vehicles, power quality enhancement, smart metering, and applications of artificial intelligence in power electronic systems.